INTERNATIONAL JOURNAL FOR NUMERICAL METHODS IN FLUIDS, VOL. 10, 125–140 (1990)

ITERATIVE STABILIZATION OF THE BILINEAR VELOCITY–CONSTANT PRESSURE ELEMENT

M. FORTIN AND S. BOIVIN

Département de Mathématiques, Université Laval, Cité Universitaire, Québec, Canada G1K 7P4

SUMMARY

Some finite element approximations of incompressible flows, such as those obtained with the bilinear velocity–constant pressure element (Q_1–P_0), are well known to be unstable in pressure while providing reasonable results for the velocity.

We shall see that there exists a subspace of piecewise constant pressures that leads to a stable approximation. The main drawback associated with this subspace is the necessity of assembling groups of elements, the so-called macro-elements', which increases dramatically the bandwidth of the system.

We study a variant of Uzawa's method which enables us to work in the desired subspace without increasing the bandwidth of the system. Numerical results show that this method is efficient and can be made to work at a low extra cost. The method can easily be generalized to other problems and is very attractive in three-dimensional cases.

KEY WORDS Incompressible flow Finite element Stability

1. INTRODUCTION

Finite element methods using isoparametric triangular or quadrilateral elements are now widely used to approximate incompressible materials. However, in order to get stable and accurate results, the approximation spaces have to satisfy the well known inf–sup (or Babuška–Brezzi) condition. It is surprising to realize, however, that one of the most popular choices of element, namely the bilinear velocity–constant pressure element (Q_1–P_0), does not satisfy this stability condition. In fact, this element is still defeating the efforts for a general proof of convergence, although numerical evidence suggests that velocity and some filtered pressure do often converge. Results from Pitkäranta and Stenberg[1] and Brezzi and Fortin[2] prove convergence on special meshes.

In this paper we present a variant of Uzawa's method which enables us to relate theory and practice by permitting us to obtain good computed velocities and pressure. To do this we use a projection on a well chosen pressure subspace, where pressure is free of any spurious mode.[3] This subspace was first considered in Johnson and Pitkäranta[4] where it was used to prove a convergence result on a regular mesh. We consider it here in a more general setting.

We shall restrict our attention to the Stokes problem and the bidimensional Q_1–P_0 element, but the method can be extended to other elements and to 3D problems, where the low number of degrees of freedom of the Q_1–P_0 element makes it attractive.

0271–2091/90/020125–16$08.00

Received 4 January 1988
Revised 17 March 1989

2. NOTATION AND PRELIMINARY RESULTS

Let Ω be a polygonal domain in $\mathbb{R}^2$, with boundary $\Gamma = \partial\Omega$. The stationary Stokes equations for an incompressible viscous fluid can be written as

$$-\nu\Delta\mathbf{u} + \operatorname{grad} p = \mathbf{f},$$

$$\operatorname{div}\mathbf{u} = g, \qquad \int_{\partial\Omega} g\,dx = 0, \tag{1}$$

$$\mathbf{u}_{|\Gamma} = 0,$$

where $\mathbf{u}$ is the fluid velocity, p is the pressure, $\mathbf{f}$ is the body force and $\nu > 0$ is the kinematic viscosity. We have introduced a general condition $\operatorname{div}\mathbf{u} = g$. Such a g is often implicitly defined by a non-homogeneous boundary condition. We shall, without loss of generality, let $\nu = 1$.

We denote $|\cdot|_{s,\Omega}$ and $\|\cdot\|_{s,\Omega}$ respectively the semi-norm and norm of the Sobolev space $(H^s(\Omega))^n$, where s and n are integers. As usual, $H_0^1(\Omega)$ denotes the subspace of $H^1(\Omega)$ consisting of functions with vanishing trace on Γ. We also introduce the following functional space:

$$L_0^2(\Omega) = \left\{ p \in L^2(\Omega) \,|\, \int_\Omega p\,dx = 0 \right\}$$

Defining the bilinear forms $a(\cdot,\cdot)$ and $b(\cdot,\cdot)$ by

$$a(\mathbf{u},\mathbf{v}) = \int_\Omega \operatorname{grad}\mathbf{u} : \operatorname{grad}\mathbf{v}\,dx,$$

$$b(\mathbf{v},q) = -\int_\Omega q \operatorname{div}\mathbf{v}\,dx,$$

problem (1) can be formulated variationally as

$$a(\mathbf{u},\mathbf{v}) + b(\mathbf{v},p) = \int_\Omega \mathbf{f}\cdot\mathbf{v}\,dx, \quad \forall\mathbf{v} \in (H_0^1(\Omega))^n,\ \mathbf{u} \in (H_0^1(\Omega))^n, \tag{2}$$

$$b(\mathbf{u},q) = (g,q), \quad \forall q \in L^2(\Omega), \quad p \in L_0^2(\Omega). \tag{3}$$

These equations are in fact the optimality conditions of the following Lagrangian:

$$\mathscr{L}(\mathbf{v},q) = \tfrac{1}{2}a(\mathbf{v},\mathbf{v}) + b(\mathbf{v},q) - \int_\Omega \mathbf{f}\cdot\mathbf{v}\,dx - \int_\Omega gq\,dx. \tag{4}$$

To $b(\mathbf{v},q)$ we associate the linear operators $B = -\operatorname{div}$ and $B^t = +\operatorname{grad}$ defined by

$$\langle B\mathbf{v}, q\rangle = \langle \mathbf{v}, B^t q\rangle = b(\mathbf{v},q), \quad \forall\mathbf{v} \in (H_0^1(\Omega))^n,\ q \in L^2(\Omega).$$

We will have to study the subspace $\ker B = \{\mathbf{v} \in (H_0^1(\Omega))^n \,|\, \operatorname{div}\mathbf{v} = 0\}$. As to $\ker B^t$, it evidently consists of constant functions.

Considering a finite element triangulation τ_h of Ω into quadrilaterals, we introduce the finite dimensional subspaces $V_h \subset (H_0^1(\Omega))^n$ and $Q_h \subset L^2(\Omega)$ defined by

$$V_h = \{\mathbf{v} \in (H_0^1(\Omega))^2 \,|\, \mathbf{v}_{|K} \in (Q_1(K))^2,\ \forall K \in \tau_h\},$$

$$Q_h = \{p \in L^2(\Omega) \,|\, P_{|K} \in P_0(K),\ \forall K \in \tau_h\},$$

where $Q_1(K)$ is the space of (isoparametrically) transformed bilinear functions[5] and $P_0(K)$ is the space of piecewise constant functions. We shall frequently refer to this discretization as the Q_1–P_0 discretization.

On these spaces, we formulate the approximate problem as: find $\mathbf{u}_h$ in V_h and p_h in Q_h such that

$$a(\mathbf{u}_h, \mathbf{v}_h) + b(\mathbf{v}_h, p_h) = \int_\Omega \mathbf{f}\cdot\mathbf{v}_h \, dx, \quad \forall \mathbf{v}_h \in V_h, \tag{5}$$

$$b(\mathbf{u}_h, q_h) = (g_h, q_h), \quad \forall q_h \in Q_h. \tag{6}$$

Here again we define the operators B_h and B_h^t by

$$\langle B_h \mathbf{v}_h, q_h\rangle = \langle \mathbf{v}_h, B_h^t q_h\rangle = b(\mathbf{v}_h, q_h), \quad \forall \mathbf{v}_h \in V_h,\ q_h \in Q_h,$$

and the subspaces $\ker B_h = \{\mathbf{v}_h \in V_h \mid B_h v_h = 0\}$ and,

$$\ker B_h^t = \{q_h \in Q_h \mid B_h^t q_h = 0\}.$$

From Brezzi,[6] stability of such a finite element approximation requires that the following inf–sup condition be satisfied for a constant k *independent of* h:

$$\inf_{q_h} \sup_{v_h \neq 0} \frac{\int_\Omega q_h \operatorname{div} \mathbf{v}_h \, dx}{\| \mathbf{v}_h \|_{V_h} \| q_h \|_{Q_h/\mathbb{R}}} \geqslant k. \tag{7}$$

The quotient norm on Q_h appears because pressure is defined up to an additive constant in problem (5),(6). Condition (7) means implicitly that the pressure must also be defined up to an additive constant in the finite dimensional case. This is not straightforward, however.

Stability of finite element approximations of incompressible materials (as defined by condition (7)) is related to the properties of the discrete divergence operator and its transpose. Usually, this operator is not the restriction of B to Q_h. In fact, $B_h u_h$ is the projection of Bu_h on the space Q_h; this is the case for the Q_1–P_0 element just introduced, where B_h is the average divergence on each element. System (5), (6) is singular and the pressure is determined only up to an additive constant for any reasonable approximation. This also implies that we have a compatibility condition on data. When a non-homogeneous Dirichlet problem is considered, this is nothing but the obvious global balance of mass

$$\int_{\partial\Omega} \mathbf{u}\cdot\mathbf{n} \, ds = 0.$$

In some discretizations, the kernel of the discrete gradient operator is more than one-dimensional. This is the case for the Q_1–P_0 approximation on a rectangular mesh where we have an extra pressure mode in the famous checkerboard pattern. Besides requiring some filtering of pressure, this also means that an extra compatibility condition has to be imposed on data. This extra condition has no physical meaning and thus imposes an artificial constraint on data.

A typical example of this is the driven cavity problem, discretized with a regular mesh of rectangular Q_1–P_0 elements. In the case of a 'flow-through' cavity, that is, with equal velocity at each node on the driven side (Figure 1(a)), the problem is well posed but will require a filtering of the pressure. In the more difficult case of a 'contained' flow in a cavity, that is, a cavity with zero velocity at each corner node and constant velocity on the driven side (Figure 1(b)), the problem is well posed for an odd number of elements on the driven side (provided that the first and last elements on the driven side have same length) but is *ill-posed for an even number of elements* on this side.[3]

We shall now see how reducing the space of discrete pressures can lead to a stable approximation. We shall then relate this fact to convergence results for the original $Q_1 - P_0$ element. Finally, we shall introduce our iterative method.

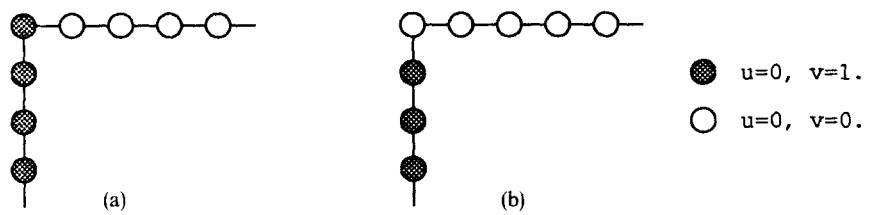

Figure 1. Boundary conditions (a) flow-through and (b) contained flow in a cavity

3. MACRO-ELEMENT TECHNIQUES AND THE Q_1–$\hat{P}_0$ ELEMENT

As we have already noted in the previous sections, a complete analysis of the Q_1–P_0 element is still not available, even after 15 years of effort. Partial results have nevertheless been found and we shall review those that will be relevant to the numerical method we want to introduce. A fundamental tool will be the notion of composite element or macro-element. We define this (see e.g. Reference 7) as a patch M of elements following a well defined pattern, i.e. that can be transformed continuously into a reference configuration $\hat{M}$. In the following we shall consider specially a macro-element M built of four arbitrary quadrilaterals as in Figure 2 and we shall suppose that our finite element mesh is built of such macro-elements. In practice, this is not a very strong restriction.

In a first step we define a subspace $\hat{Q}_h \subset Q_h$ such that the discrete problem in $V_h \times \hat{Q}_h$ is stable. To do so we define[4] an orthogonal basis of Q_h using the macro-element M. Let A_i denote the area of element K_i of M. We take $\phi_{j,M}$ to be the piecewise constant functions schematized in Figure 3.

Then we define

$$\hat{Q}_h = \left\{ \sum_M \left[\sum_{i=1}^{3} \alpha_{iM} \phi_{i,M} \right] \right\}, \qquad \tilde{Q}_h = \left\{ \sum_M \alpha_{4M} \phi_{4,M} \right\}. \tag{8}$$

A checkerboard mode will obviously take its roots in $\tilde{Q}_h$. It is also clear, by construction, that $\tilde{Q}_h$ and $\hat{Q}_h$ are orthogonal with respect to the $L^2(\Omega)$ scalar product. We thus define

$$P_{\tilde{Q}h} p_h = \sum_M \alpha_{4M}(p_h) \phi_{4,M}, \tag{9}$$

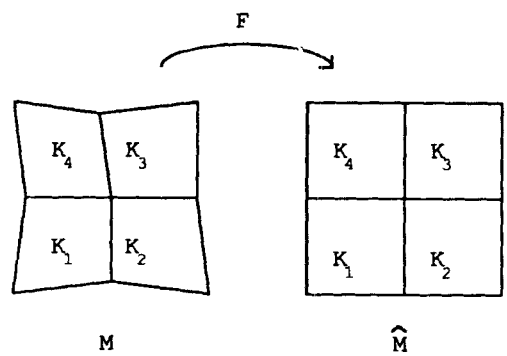

Figure 2. A macro-element M and its reference $\hat{M}$

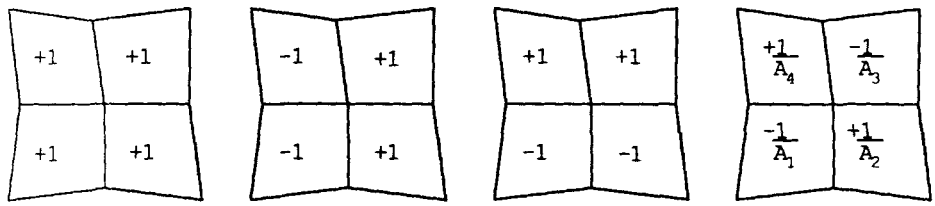

(a) $\phi_{1,M}$ (b) $\phi_{2,M}$ (c) $\phi_{3,M}$ (d) $\phi_{4,M}$

Figure 3. Pressure basis on M

where

$$\alpha_{4M}(P_h)=\frac{\int_M P_h\phi_{4,M}\,dx}{\int_M \phi_{4,M}\phi_{4,M}\,dx} \tag{10}$$

and $P_{\hat{Q}_h}p_h=(I-P_{\hat{Q}_h})p_h=p_h-\sum_M \alpha_{4,M}(p_h)\phi_{4,M}$.

Let us now consider a new element defined on M by using V_h as the space of velocities and $\hat{Q}_h$ for pressure. On the macro-element considered there is exactly the same number of degrees of freedom as the Q_2–P_1 element and a stability proof can be given.[8] There is no advantage in using explicitly this element, however, since we only get O(h) convergence for a bandwidth and general complexity similar to that of the Q_2–P_1 case. Degrees of freedom of this *new element*, which we denote Q_1–$\hat{P}_0$, are schematically represented in Figure 4 throughout the corresponding degrees of freedom.

The above results are easily extended to the three-dimensional case. We now have $3n-2$ unstable modes to eliminate on a cube of $n \times n \times n$ cubic Q_1–P_0 elements. If we assume that the mesh is divided into a $2 \times 2 \times 2$ macro-element (Figure 5), four modes have to be eliminated. The first mode of Figure 5 is the only genuine 3D mode while the other three are symmetries of 2D modes.

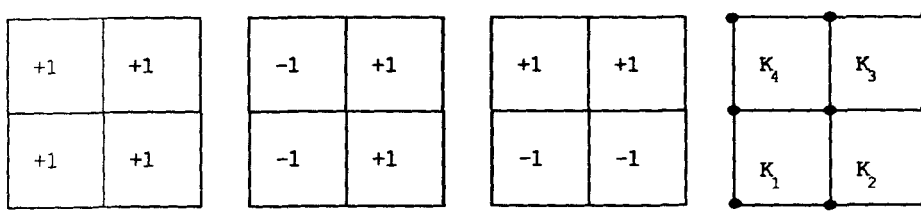

(a) $\phi_{1,M}$ (b) $\phi_{2,M}$ (c) $\phi_{3,M}$ (d) Velocity nodes

Figure 4. Degrees of freedom of the Q_1–$\hat{P}_0$ element

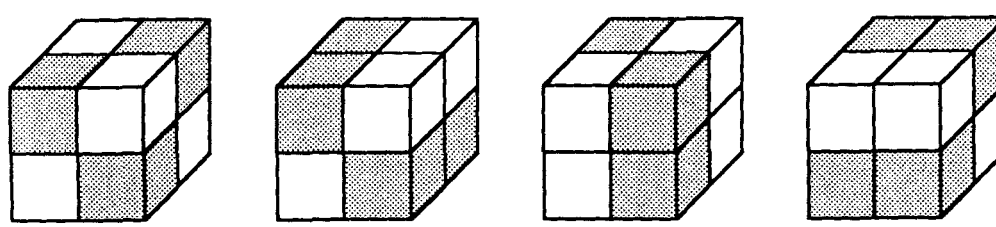

(a) (b) (c) (d)

Figure 5.

Now we have a stable element, leading to an $O(h)$ convergence, which is isomorphic to the Q_2–P_1 element, thus implying almost the same cost. In order to reduce the cost to the level of the standard Q_1–P_0 element, we will iteratively correct the computed pressure from the Q_1–P_0 element in order to insure that the pressure stays in the right space. This is achieved by projecting, at each iteration, the pressure on the space generated by the degrees of freedom of $\hat{Q}_h$.

Before presenting our algorithm, it may be worth showing how the above construction is related to the convergence of the standard Q_1–P_0 element. In fact, we recall that according to the results of Johnson and Pitkäranta[4] it is possible to prove convergence of the Q_1–P_0 element on a regular mesh. More precisely, what can be obtained is an error estimate on $\|u-u_h\|$ and $\|p-\hat{p}_h\|$ with $\hat{p}_h = P_{\hat{Q}_h} p_h$. This result has been extended by Pitkäranta and Stenberg[1] to the case of a general mesh formed by a 4×4 regularly partitioned macro-element (Figure 6).

However, no result is known (up to now) for a completely general mesh. A proof of the results quoted above can also be found in Reference 2.

4. TWO ITERATIVE IMPLEMENTATIONS OF THE Q_1–$\hat{P}_0$ ELEMENT

The finite dimensional problem (5), (6) can be conveniently rewritten as (with subscript h and 'bold' notation dropped)

$$Au + B^t p = f, \tag{11}$$

$$Bu = g, \tag{12}$$

where $A \in \mathscr{L}(\mathbb{R}^N, \mathbb{R}^N)$, $B \in \mathscr{L}(\mathbb{R}^N, \mathbb{R}^M)$, $u \in \mathbb{R}^N$, $g \in \mathbb{R}^M$ and $p \in \mathbb{R}^M$.

A basic technique used to solve such a problem is Uzawa's method applied to the following augmented Lagrangian:[9]

$$\mathscr{L}_r(v, q) = \tfrac{1}{2}(Av, v) - (f, v) + (q, Bv - g) + (r/2)|Bv - g|^2, \tag{13}$$

which can be written as follows.

Uzawa's method

Let $p^0 \in \mathbb{R}^M$ be chosen arbitrarily, say $p^0 = 0$; we construct p^{n+1} and u^n from p^n by induction as

$$\mathscr{L}_r(u^n, p^n) \leqslant \mathscr{L}_r(v, p^n), \quad u^n \in V_h, \quad \forall v \in V_h, \tag{14}$$

$$p^{n+1} = p^n + \rho(Bu^n - g), \quad 0 < \rho < 2r, \tag{15}$$

We note that (14) is equivalent to

$$(A + rB^t B)u^n + B^t p^n = f + rB^t g. \tag{16}$$

A complete analysis of this algorithm can be found in Reference 9, where the choice of r is also extensively discussed.

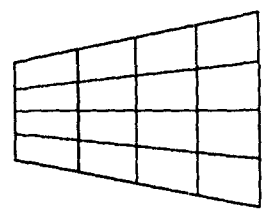

Figure 6. A typical 4×4 macro-element

Before introducing our new method we recall an algorithm based on the saddle point technique to implement the Q_1–$\hat{P}_0$. This was previously discussed in Reference 10. Here we consider $Pp=0$ as a new constraint on the system (11), (12) and we consider the following Lagrangian.

$$\mathcal{L}(v,q,\lambda)=\tfrac{1}{2}(Av,v)-(f,v)+(q,Bv-g)+(\lambda,Pp).$$

To find a saddle point of $\mathcal{L}$ we apply the classical Uzawa algorithm:

let $\lambda^0 \in \mathbb{R}^M$ be chosen arbitrarily;

λ^n being known, solve for u^n, p^n,

$$\inf_v \sup_q \mathcal{L}(v,q,\lambda^n);$$

then update the dual variable λ by $\lambda^{n+1}=\lambda^n+\rho Pp^n$.

Using a conjugate gradient method to implement the above algorithm, we find the following.

Conjugate gradient algorithm

1. Choose λ^0 arbitraily, possibly 0.
2. λ^0 being given, solve the following Stokes problem:

$$Au^0+B^tp^0=f,$$

$$Bu^0=\lambda^0.$$

3. p^n being given, solve the following Stokes problem:

$$Aw^n+B^tz^n=0,$$

$$Bw^n=Pp^n.$$

4. Compute

$$\beta^n=\frac{-(Pz^n,\phi_\lambda^n)}{(P\phi_p^n,\phi_\lambda^n)}.$$

5. Update the new descent directions by

$$\phi_u^{n+1}=w^n+\beta^n\phi_u^n,$$

$$\phi_p^{n+1}=z^n+\beta^n\phi_p^n,$$

$$\phi_\lambda^{n+1}=Pp^n+\beta^n\phi_\lambda^n.$$

6. Compute

$$\rho^n=\frac{-(Pz^n,\phi_\lambda^{n+1})}{(P\phi_p^{n+1},\phi_\lambda^{n+1})}.$$

7. Update the variables by

$$u^{n+1}=u^n+\rho^n\phi_u^{n+1},$$

$$p^{n+1}=p^n+\rho^n\phi_p^{n+1},$$

$$\lambda^{n+1}=\lambda^n+\rho^n\phi_\lambda^{n+1}.$$

8. Stop if $|Pp^n|^2<\varepsilon$, else go to step 3. □

This algorithm has proved to work well (see Reference 10) and the next section) and will serve as a basis to compare the next algorithm to be described, namely the prorojected Uzawa algorithm. To introduce this new algorithm we recall the genuine algorithm based on the direct, and costly, use of the Q_1–$\hat{P}_0$ element.

Working directly in the space $\hat{Q}_h$ can be viewed as working with the following Lagrangian and the associated Uzawa algorithm:

$$\mathscr{L}_r(v, q)=\tfrac{1}{2}(Av, v)-(f, v)+(q,(I-P)(Bv-g))+(r/2)|(I-P)(Bv-g)|^2, \tag{17}$$

where P: $Q_h \to \tilde{Q}_h$ and $(I-P)$: $Q_h \to \hat{Q}_h$ are the projection operators defined in Section 3. This would imply an assembly on the macro-elements which dramatically increases the bandwidth of the system to be solved. To avoid this problem we will make use of the approximation

$$(I-P)Bu^n \approx Bu^n - PBu^{n-1}, \tag{18}$$

which enables us to write Uzawa's algorithm in the following weaker form.

Projected Uzawa method

Let $u^{-1} \in \hat{V}_h$ and $p^0 \in \hat{Q}_h$ be chosen arbitrarily;
given u^{n-1} and p^n, we find u^n and p^{n+1} by solving

$$(A+rB^tB)u^n - rB^tPBu^{n-1} + B^tp^n = f + rB^t(I-P)g, \tag{19}$$

$$p^{n+1} = p^n + \rho(I-P)(Bu^n - g), \quad 0<\rho<2r. \tag{20}$$

Before illustrating the use of this algorithm numerically, we need to check the validity of hypothesis (18). In fact, we prove the convergence of algorithm (19), (20).

Theorem 1

For $0<\rho<2r$ and for all $u^{-1} \in \hat{V}_h$, $p^0 \in \hat{Q}_h$ we have

$$|u^n - u| \to 0, \qquad |(I-P)Bu^n - (I-P)Bu| \to 0,$$

$$|p^n| \leqslant M_1, \qquad |p^{n+1} - p^n| \to 0,$$

$$|PBu^n| \leqslant M_2, \qquad |PBu^{n+1} - PBu^n| \to 0. \qquad \square$$

Proof. Let $\{u, p\}$ be a saddle point of $\mathscr{L}_r$. This point is characterized by

$$(A+rB^tB)u - rB^tPBu + B^tp = f + rB^t(I-P)g, \tag{21}$$

$$(I-P)Bu = g \Leftrightarrow p = p + \rho(I-P)(Bu-g). \tag{22}$$

Let us introduce $\bar{u}^n = u^n - u$, $\bar{p}^n = p^n - p$. By subtracting (21) from (19) and (22) from (20) we find

$$(A+rB^tB)\bar{u}^n - rB^tPB\bar{u}^{n-1} + B^t\bar{p}^n = 0, \tag{23}$$

$$\bar{p}^{n+1} = \bar{p}^n + \rho(I-P)B\bar{u}^n. \tag{24}$$

Then, multiplying (24) by $\bar{p}^{n+1}$ and (23) by $\bar{u}^n$ we deduce

$$\frac{1}{2\rho}|\bar{p}^{n+1}|^2 - \frac{1}{2\rho}|\bar{p}^n|^2 + \frac{1}{2\rho}|\bar{p}^{n+1} - \bar{p}^n|^2 - ((I-P)B\bar{u}^n, \bar{p}^{n+1} - \bar{p}^n) - ((I-P)B\bar{u}^n, \bar{p}^n) = 0, \tag{25}$$

$$(A\bar{u}^n, \bar{u}^n) + r((I-P)B\bar{u}^n, B\bar{u}^n) + r(PB\bar{u}^n - PB\bar{u}^{n-1}, B\bar{u}^n) + (\bar{p}^n, B\bar{u}^n) = 0. \tag{26}$$

As operators, P and $(I-P)$ are orthogonal, so we can write

$$((I-P)B\bar{u}^n, B\bar{u}^n)=|(I-P)B\bar{u}^n|^2,$$

$$(PB\bar{u}^n - PB\bar{u}^{n-1}, B\bar{u}^n) = (PB\bar{u}^n - PB\bar{u}^{n-1}, PB\bar{u}^n)$$

$$= \tfrac{1}{2}|PB\bar{u}^n|^2 - \tfrac{1}{2}|PB\bar{u}^{n-1}|^2 + \tfrac{1}{2}|PB\bar{u}^n - PB\bar{u}^{n-1}|^2, \tag{27}$$

$$(\bar{p}^n, B\bar{u}^n)=(\bar{p}^n, (I-P)B\bar{u}^n).$$

Substituting relations (27) in (25), (26) and adding the last two we get

$$(A\bar{u}^n,\bar{u}^n)+r|(I-P)B\bar{u}^n|^2+\frac{r}{2}|PB\bar{u}^n|^2-\frac{r}{2}|PB\bar{u}^{n-1}|^2+\frac{r}{2}|PB\bar{u}^n-PB\bar{u}^{n-1}|^2$$

$$+\frac{1}{2\rho}|\bar{p}^{n+1}|^2-\frac{1}{2\rho}|\bar{p}^n|^2+\frac{1}{2\rho}|\bar{p}^{n+1}-\bar{p}^n|^2-((I-P)B\bar{u}^n, \bar{p}^{n+1}-\bar{p}^n)=0. \tag{28}$$

Using the estimate

$$((I-P)B\bar{u}^n, \bar{p}^{n+1}-\bar{p}^n) \leqslant \frac{\varepsilon}{2}|(I-P)B\bar{u}^n|^2+\frac{1}{2\varepsilon}|\bar{p}^{n+1}-\bar{p}^n|^2$$

and the ellipticity of A we deduce from (28) that

$$\alpha|\bar{u}^n|^2+\left(r-\frac{\varepsilon}{2}\right)|(I-P)B\bar{u}^n|^2+\frac{r}{2}|PB\bar{u}^n|^2-\frac{r}{2}|PB\bar{u}^{n-1}|^2+\frac{r}{2}|PB\bar{u}^n-PB\bar{u}^{n-1}|^2$$

$$+\frac{1}{2\rho}|\bar{p}^{n+1}|^2-\frac{1}{2\rho}|\bar{p}^n|^2+\left(\frac{1}{2\rho}-\frac{1}{2\varepsilon}\right)|\bar{p}^{n+1}-\bar{p}^n|^2\leqslant 0. \tag{29}$$

Finally, adding the N equations of type (29) we get

$$\alpha\sum_1^N|\bar{u}^n|^2+\left(r-\frac{\varepsilon}{2}\right)\sum_1^N|(I-P)B\bar{u}^n|^2+\frac{r}{2}|PB\bar{u}^n|^2+\frac{r}{2}\sum_1^N|PB\bar{u}^n-PB\bar{u}^{n-1}|^2$$

$$+\frac{1}{2\rho}|\bar{p}^{N+1}|^2+\left(\frac{1}{2\rho}-\frac{1}{2\varepsilon}\right)\sum_1^N|\bar{p}^{n+1}-p^n|^2\leqslant\frac{r}{2}|PB\bar{u}^0|^2+\frac{1}{2\rho}|\bar{p}^0|^2. \tag{30}$$

Choosing $0<\rho\leqslant\varepsilon<2r$, the left hand part of (30) is a monotonic, increasing, bounded sequence, hence convergent. As each sum has to be convergent, the terms $|\bar{u}^n|^2$, $|(I-P)B\bar{u}^n|^2$, $|PB\bar{u}^n-PB\bar{u}^{n-1}|^2$ and $|\bar{p}^{n+1}-\bar{p}^n|$ have to converge to zero. This completes the proof. □

An improved algorithm comes from the following observation: Owing to the explicit form of the term $(I-P)Bu$ (see equation (18), the first iteration of the algorithm will force PBu to become small, and since PBu is the feedback control on the oscillations, the smaller its value the smaller the correction. The new 'relaxed' form of the projected Uzawa algorithm is

let $u^{-1}\in\hat{V}_h$ and $p^0\in\hat{Q}_h$ be chosen arbitrarily;
then let $\lambda^0=PBu^{-1}$;
given u^{n-1}, p^n and λ^n, we find u^n, p^{n+1} and λ^{n+1} by solving

$$(A+rB^tB)\delta u^n=f-Au^{n-1}-rB^t(Bu^{n-1}-g)+rB^t\lambda^n-B^tp^n, \tag{31}$$

$$u^n=u^{n-1}+\delta u^n, \tag{32}$$

$$p^{n+1}=p^n+\rho(I-P)(Bu^n-g), \quad 0<\rho<2r, \tag{33}$$

$$\lambda^{n+1} = \lambda^n + \beta(I - P)(PBu^{n+1} - \lambda^n). \tag{34}$$

In practice, $\beta = 2$ appeared to be a good choice.

Convergence of this algorithm can be proved along the same lines as in Theorem 1.

5. NUMERICAL RESULTS

The conjugate gradient and the modified Uzawa algorithms presented in the previous sections were both introduced in a code solving the Stokes problem by a penalty method and using the Q_1–P_0 element. Projection operators are defined as before. We suppose that the macro-element mesh has been already constructed, possibly by mesh refinement. Numericals simulations on the driven cavity problem and a flow in a distorted convergent show that these methods are efficient and provide a good approximation of velocities as well as pressure.

All our results were compared with reference solutions obtained from a well tested finite element code using the Q_2–P_1 element. The graphical results presented here came from any of the stabilization methods we have presented since all the results have error less then 1/1000.

Perturbated driven cavity

The mesh of a typical 10×10 element flow-through cavity was perturbated by displacing an internal node by 10^{-4} in each direction, producing a crude checkerboard. After a few iterations of the new algorithm, the checkerboard modes had disappeared. The result differed only slightly from the reference result, i.e. that obtained with the Q_2–P_1 element, which is free of any spurious mode.

We obtained similar results for the much more difficult case of the contained flow in a cavity, that is with zero velocities at each corner node. This problem is well known to be illposed on the original Q_1–P_0 pressure space for the square cavity with an even number of elements on the driven side.[3] Using our algorithms, however, we were able to obtain a coherent solution in a few steps (Figures 7(a) and 7(b)). It must be noted that in this contained flow problem the velocity field is oscillating in the neighbourhood of the corners, even for the well posed, odd number of elements case. Our iteration not only provides a solution in the even and odd cases but the solution is a smooth one.

Distorted convergent

Another significant example is the distorted convergent of Figures 8(a) and 8(b). This can be taken as an (artificial) example of a mesh on which no convergence proof is available for the standard Q_1–P_0 element and on which filtering of spurious modes is much harder than in the first case. A parabolic profile is imposed at the entrance and at the exit in such a way as to conserve the flow. Here again a crude checkerboard appears (Figure 8(a)). A few iterations of the new algorithm are enough to remove most of the checkerboard mode (Figure 8(b)). The result differs only slightly from the reference result which is free of any spurious mode.

Velocities

In the above cases the velocities after a few iterations differ only slightly from those obtained without filtering (Figure 10). This fact seems to be general on a fine mesh. However, for complex flow relative to the mesh the velocities computed with Q_1–P_0 can be different from those computed after filtering.

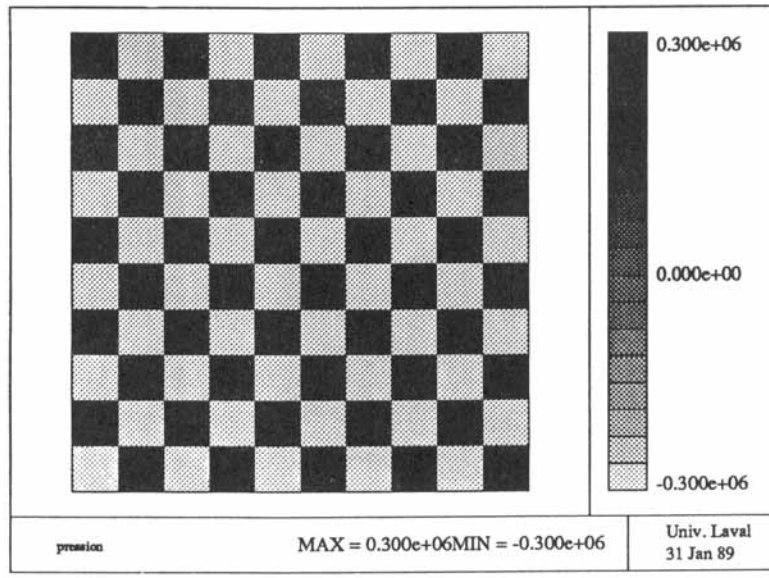

(a)

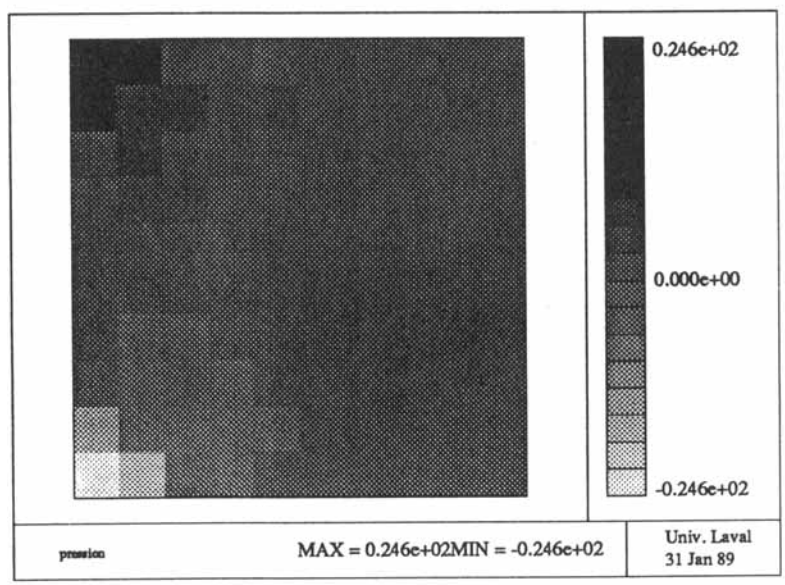

(b)

Figure 7. (a) Spurious and (b) filtered pressure in a contained flow cavity

Other numerical experiments and convergence

Rates of convergence of the factors $\|PB(u^n - u^{n-1})\|_\infty$ and $\|(I-P)Bu^n\|_\infty$ for the projected Uzawa algorithm for the difficult contained flow problem in a cavity (Figure 11) illustrate the difficulties associated with high values of r, but show also the efficiency of the method.

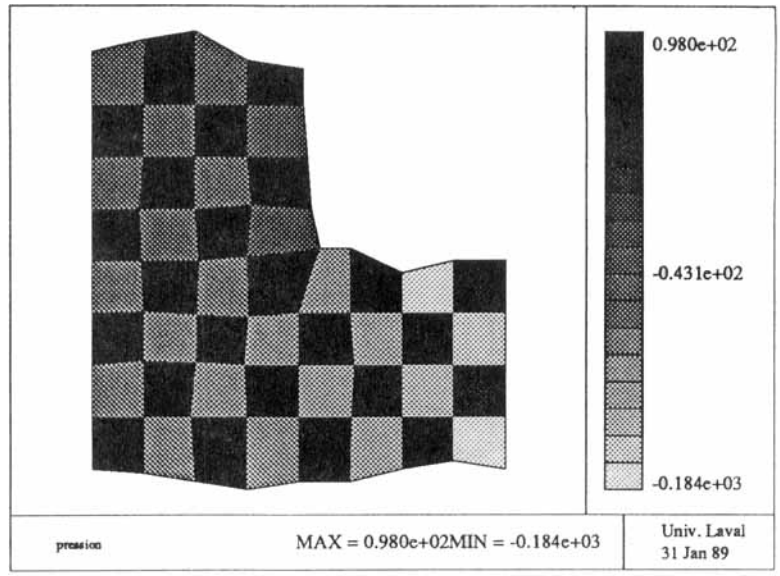

(a)

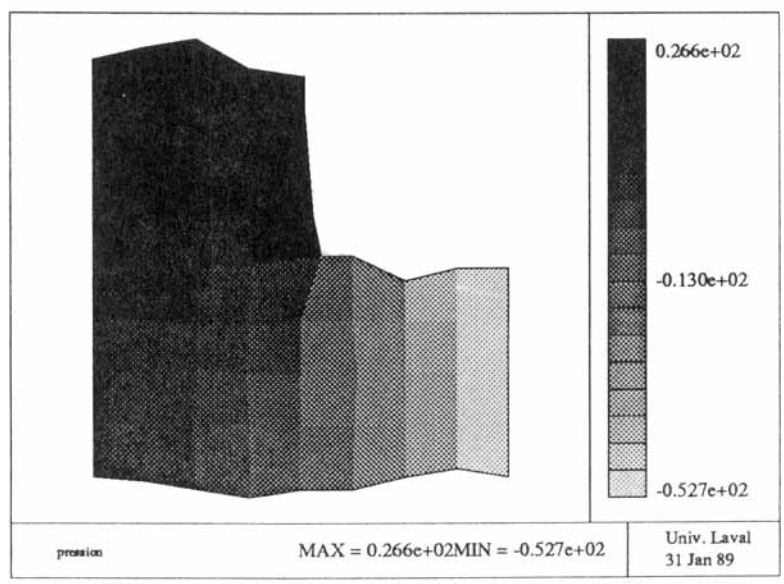

(b)

Figure 8. (a) Spurious and (b) filtered pressure in a convergent

Rates of convergence of the factor $\| Pp^n \|_\infty$ for the conjugate gradient algorithm for the difficult contained flow problem in a cavity and for the distorted convergent (Figure 12) illustrate the difficulties associated with large number of degrees of freedom, but show also the efficiency of the method.

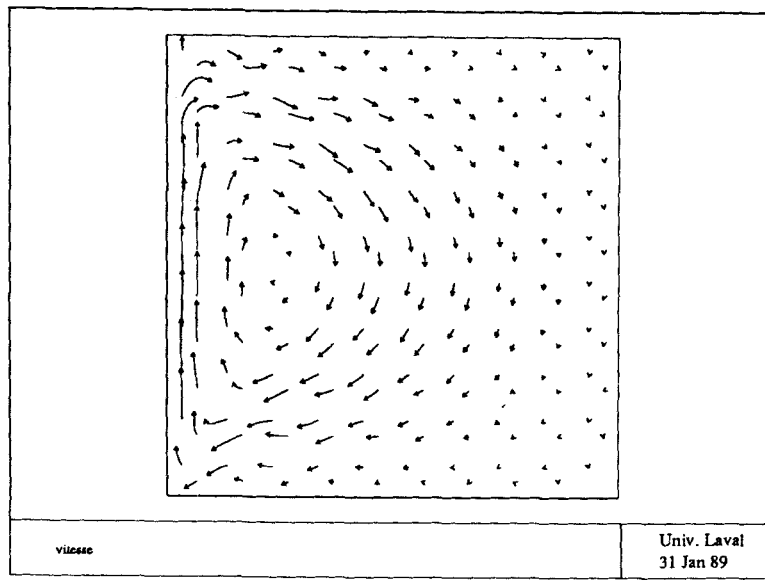

(a)

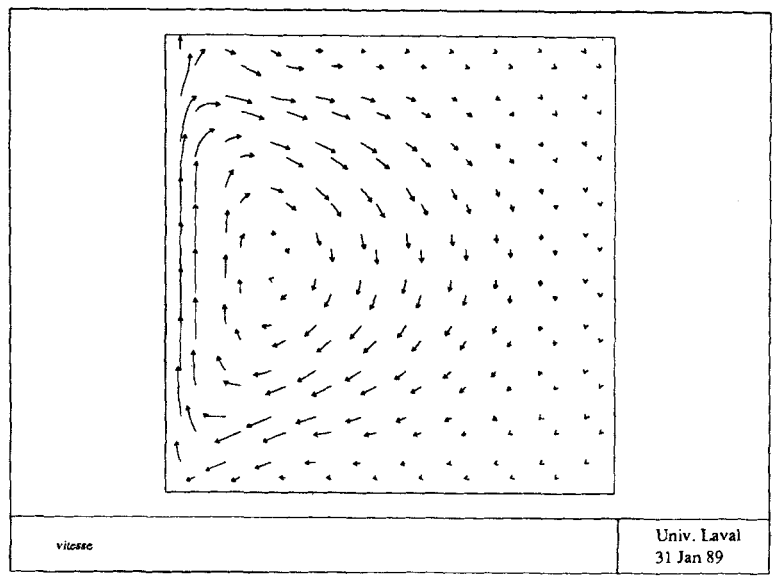

(b)

Figure 9. Contained flow in a cavity (a) before and (b) after filtering

Various combinations of the above geometries and boundary conditions have been tested and almost all showed similar convergence rates.

Regularity of the partition within each macro-element seems to be unrelated to the convergence of this algorithm.

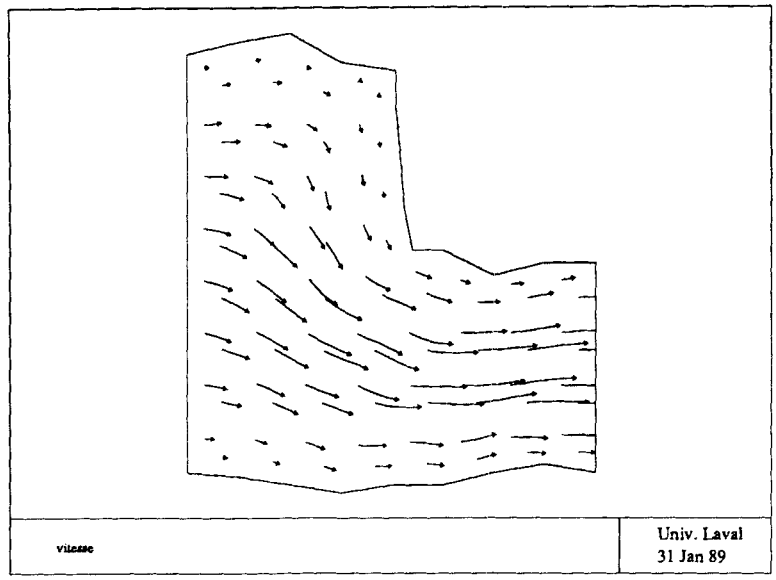

(a)

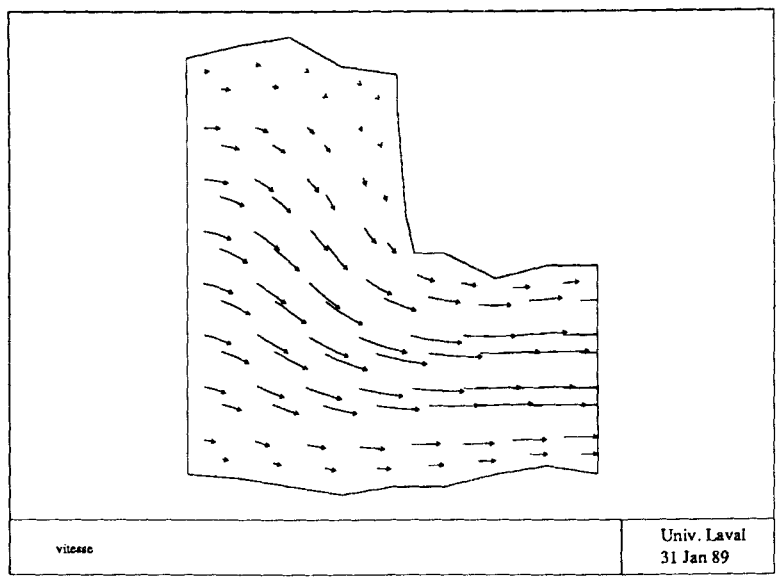

(b)

Figure 10. Flow in a convergent (a) before and (b) after filtering

6. CONCLUSIONS

We have described a new method for filtering the pure and *impure* checkerboard mode which enables us to use properly the Q_1–P_0 element. One of its advantages is that it can easily be added to an existing code without increasing the number of degrees of freedom or the bandwidth of the

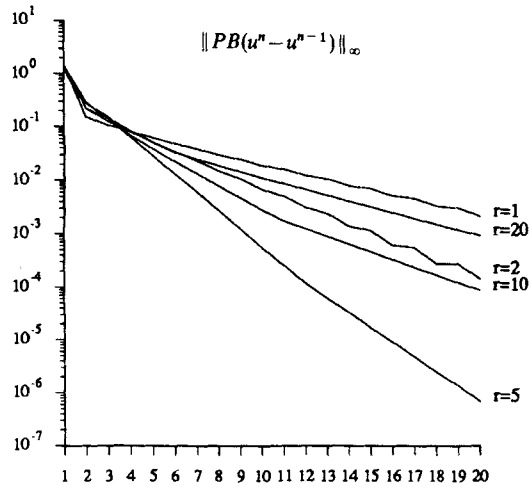

Figure 11. Convergence rates of the projected Uzawa algorithm

system. This method has been shown to perform well in 2D and can be generalized in 3D. In that case four modes have to be filtered on each macro-cube of eight hexahedral elements. Although developed for the Q_1–P_0 element and the Stokes problem, it can be modified for other pressure-unstable elements and for non-linear problems, where it can be imbedded in other iterative procedures.

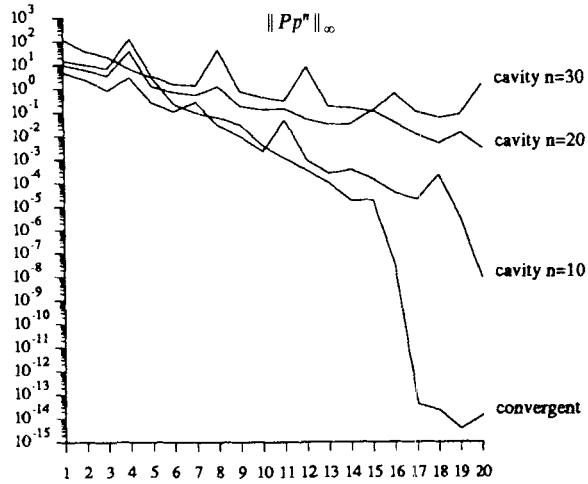

Figure 12. Convergence rates of the conjugate gradient algorithm

REFERENCES

1. G. Pitkäranta and R. Stenberg, 'Error bounds for the approximation of the Stokes problem using bilinear–constant elements on irregular quadrilateral meshes', *University of Helsinki, Report MAT-A 222*, 1984.
2. F. Brezzi, and M. Fortin, *Mixed and Hybrid Finite Element Methods*, (to appear).
3. R. L. Sani, R. M. Gresho, R. L. Lee and D. F. Griffiths, 'The cause and cure (?) of the spurious pressures generated by certain FEM solutions of the incompressible Navier–Stokes equations: Part 1', *Int. j. numer. methodssds fluids*, **1**, 17–43 (1981).
4. C. Johnson and G. Pitkäranta, 'Analysis of some mixed finite element methods related to reduced integration', *Math. Comput.*, **38**, 375–400 (1982).
5. P. G. Ciarlet, *The Finite Element Method for Elliptic Problems*, North-Holland, Amsterdam, 1978.
6. F. Brezzi, 'On the existence, uniqueness and approximation of saddle point problems arising from Lagrange multipliers', *R.A.I.R.O.*, **R2**, 123–151 (1974).
7. R. Stenberg, 'Analysis of finite element methods for the Stokes problem: a unified approach', *Math. Comput.* **42**, 9–33 (1984).
8. M. Fortin, 'An analysis of the convergence of mixed finite element methods', *R.A.I.R.O.*, **11**, 341–354 (1977).
9. M. Fortin and R. Glowinski, *Augmented Lagrangian Methods: Application to the Numerical Solution of Boundary-value Problems*, North-Holland Amsterdam, 1983.
10. M. Fortin, and S. Boivin 'A stabilization method for some finite element approximations of incompressible flows', *Numerical Methods in Laminar and Turbulent Flow*, Pineridge Press, Swansea, 1987.